Science Press

ARTICLE

Microstructure, Martensitic Transformation and Magnetocaloric Effect of $Ni_{50-x}Co_xMn_{39}Sn_{11}$ Heusler Alloy Ribbons

Zhang Mingang[1],   Li Shaobo[1],   Chen Fenghua[1],   Zhang Wen[1],   Li Fan[1],

Xu Xiaohong[2],   Liu Jiansheng[1]

[1]Taiyuan University of Science and Technology, Taiyuan 030024, China; [2] Shanxi Normal University, Linfen 041004, China

Abstract: A series of $Ni_{50-x}Co_xMn_{39}Sn_{11}$ (x=0~8) alloy ribbons were prepared by single-roll melt spinning method, and its crystal structure, phase transition, and magnetocaloric effect were investigated. The results show that martensitic transformation temperatures decrease rapidly and the Curie temperature of austenite phase increases monotonously with the replacement of Ni with Co. The structural transformation can be induced not only by the temperature but also by the magnetic field. Under a magnetic field strength of 2400 kA/m, a large magnetic entropy change and a refrigerant capacity are achieved with much lower hysteresis loss in the heating and cooling processes.

Key words: Ni-Co-Mn-Sn alloy; martensitic transformation; magneto-caloric effect; magnetic entropy change

Solid refrigeration materials have received increasing attention due to the potentials of eliminating ozone, depleting gas emissions, and high cooling efficiency compared with the conventional gas refrigeration. These magnetic materials are also looked up as an economically viable option for domestic and industrial refrigeration.

The large magneto-caloric effect (MCE) was discovered in 1881[1]. However, two major developments occurred in 1997. The invention of the magnetic refrigerator demonstrates that magnetic refrigeration is a viable and competitive cooling technology in the near room temperature region, which can potentially save energy by up to 30%. The second breakthrough was the announcement of the discovery of the giant MCE in $Gd_5(Si_2Ge_2)$, which offered a promising development of economical and environmentally friendly magnetic refrigerants working near room temperature[2]. The traditional magnetic refrigeration alloy mainly

refers to some paramagnetic materials without martensitic structural transformation (MST) such as $MnFeP_{1-x}As_x$, Gd_5-$(Si_xGe_{1-x})_4$, $MnAs_{1-x}Sb$, and $La(Fe_xSi_{1-x})_{13}$[3-6]. In recent years, as a new kind of multifunctional material, the investigation has been focused on the Ni-Mn-X (X=Ga, In, Sn, Sb) ferromagnetic shape memory alloys (FSMAs), and the related intermetallic compounds with partial substitution of Al, Ti, Cr, Fe, Co, Gu, Ge, Pb etc for Ni/Mn[7-21]. The extensively potential application in magnetic refrigerant, sensor, and actuator is due to the strong coupling between the crystal structure and magnetism. During the cooling process, these alloys first undergo a pure magnetic transition at the Curie temperature of austenitic phase (T_C^A), and then experience a martensitic transformation (MT) from a high temperature austenitic phase with L21 structure to a low temperature martensitic phase with lower symmetry upon cooling procedure. Simultaneously, a large magnetization

difference (ΔM) was obtained during the MT in some alloys with specific composition. So we can speculate on a large Zeeman energy $H\Delta M$ between the two phases of the above alloys, which can drive a field induced reverse martensitic transformation (RMT). MT is one kind of solid-state first-order structural phase transformation, with displacement, non-diffusing, and dominated by the strain-energy arising from shear-like displacements[22].

In the case of Ni$_2$MnSn alloy, it has a cubic L21 structure, which has no ferromagnetic transition upon cooling and heating. Up to now, most of the researchers have focused on these off-stoichiometric Ni$_2$Mn$_{1+x}$Sn$_{1-x}$ alloys owing to the combination of its MST and magnetic transition property. In these alloys, the content of Mn is less than that of Ni. Excess Mn atoms would occupy the vacant Sn sites, and the magnetic coupling between the Mn atoms on Sn sites and the Mn atoms on regular Mn sites is antiferromagnetic. As we know, the structural and magnetic properties of the Ni-Mn-Sn based FSMAs are very sensitive to the composition, due to the strong dependence of MT temperature on the valence electron concentration per atom (e/a) [23] and Mn-Mn interatomic distances[24]. So the most useful methods up to now to tune MT temperatures (M_s, A_s, and A_1) and T_C^A into target temperature (including room temperature) are changing the chemical compositions of element [25-27] or doping other element[8-22]. Besides changing the composition, external factors such as preparation condition[28], annealing[11] and external parameters (magnetic field and hydrostatic pressure)[29] can also influence the magneto-structural transformation and the related physical properties strongly.

In the present work, we fabricated the Ni$_{50-x}$Co$_x$Mn$_{39}$Sn$_{11}$ (x=0, 2, 3, 4, 5, 6, 7, 8) ribbons by melt spinning. We investigated the effect of the replacement of Ni with Co on the phase transition and MCE. Our results demonstrated that both the transition temperature and MCE are strongly dependent on Co concentration.

1　Experiment

The as-cast ingots of nominal composition Ni$_{50-x}$Co$_x$Mn$_{39}$ Sn$_{11}$(x=0, 2, 3, 4, 5, 6, 7, 8) were prepared by Ar arc melting from pure elements (99.98%). To make sure a good composition homogenization, the as-cast ingots were re-melted four times. The samples were prepared by melt-spinning in an argon atmosphere at a surface velocity of 10 m/s. Microstructure of the samples was investigated by field emission scanning electron microscopy (FE-SEM, Hitachi S-4800) setup. The composition of elaborate ribbons was confirmed by X-ray energy dispersive spectrometry (EDS, Thermo System 7). Cubic L2$_1$ structures and 7M martensitic structures of the alloys were analyzed using X-ray diffractometer with Cu Kα radiation (XRD, PANalytical X'Pert PRO) at room temperature. MT

temperatures were measured by differential scanning calorimetry (DSC, 200F3 Maia) at a heating/cooling rate of 5 K/min. The magnetic properties were measured using a Quantum Design's multiple vibrating sample magnetometer VersaLab system under a magnetic field up to 2400 kA/m. Instrument temperature measurement range was 50~400 K. The magnetization M-T curves were obtained at a cooling/heating rate of 3 K/min. The magnetic field was applied along the ribbon length direction to minimize the demagnetization effect.

2　Results and Discussion

XRD patterns of Ni$_{50-x}$Co$_x$Mn$_{39}$Sn$_{11}$ (x=0, 2, 3, 4, 5, 6, 7, 8) alloys shown in Fig.1 were recorded at room temperature. Ribbons with x=0~5 exhibit a single martensite phase, which indicates that the MT temperature is below room temperature. When Co content is increased to 6%, in addition to the diffraction peaks of martensite, some other diffraction peaks belonging to austenite can also be identified in the XRD pattern. With further increasing the Co doping, ribbons fully transform into a single austenite with a cubic L21 structure at room temperature. Thus, the increase of Co content tends to enhance the stability of austenite. It is noted that there are several diffraction peaks of martensite within the 2θ range of 40°~45° in the XRD pattern, suggesting that the martensite might be modulated type. Through comparing the results reported by Krenke et al[25], modulated 7M martensite was found in the samples with x=0~6 at room temperature.

Typical SEM images of the free surface is shown in Fig.2a, and the fractured cross-section for Ni$_{50-x}$Co$_x$-Mn$_{39}$Sn$_{11}$(x=0~5) ribbon at room temperature is shown in Fig.2b. Continuous martensitic plates in Fig.2a can be ascribed to the small difference in grain orientation and dislocation substructures in adjacent grains[10]. The thickness
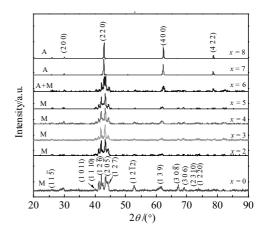

Fig.1　XRD pattern of Ni$_{50-x}$Co$_x$Mn$_{39}$Sn$_{11}$(x=0~8) melt-spun ribbons at room temperature

of the plate-shaped martensite is about 200~300 nm. As shown in Fig.2b, small equiaxed grains crystallize in a thin layer on the copper wheel side. Further, they change abruptly into an ordered columnar microstructure with a thickness of 30~40 μm. It is known that the cooling rate for the ribbon surface in contact with the copper wheel is apparently higher than that of the free surface. On the other hand, the radial direction of the copper wheel is a main heat transfer direction or thermal gradient direction during rapid solidification process for the melt-spinning, which results in the longer axis of the columnar grains to be aligned perpendicular to the ribbon plane surface[30], which is beneficial for improving the magnetic properties of the alloy.

Fig.3a shows the representative DSC curves of $Ni_{50-x}Co_x$ $Mn_{39}Sn_{11}$ (x=0, 3, 5, 7) ribbons over the temperature range between 180 K and 470 K. The large exothermic (endothermic) peak corresponds to the MT (RMT). In the DSC curves, T_C^A of ribbons with x=2~5 is masked by the intense peak associated with first order structural transition because T_C^A is too close to the MST temperatures. Therefore, it is worth noting that T_C^A is determined from the M-T curves. Fig.3b presents the Co dependence of MT temperatures (M_s, M_f, A_s, A_f) and T_C^A. It can be seen that the MT temperatures are very sensitive to the composition. The MT temperature of $Ni_{50-x}Co_xMn_{39}Sn_{11}$ (x=0~8) alloys decreases with increasing the content of Co, while T_C^A almost linearly increases. It is known that the valence electron concentration (e/a) can effectively influence the MT temperatures in

Heusler alloys[31]. Here we suppose that the valence electrons are 10 ($3d^84s^2$) for Ni, 9 ($3d^74s^2$) for Co, 7 ($3d^54s^2$) for Mn, and 4 ($5s^25p^2$) for Sn. The replacement of Ni with Co results in the decrease of the valence electron number, which leads to the decrease of MT temperatures.

Fig.4 shows the temperature dependence of magnetization (M-T) curves of $Ni_{50-x}Co_xMn_{39}Sn_{11}$ (x=0~8) alloy in a magnetic field of 8 kA/m during the heating and cooling processes. As shown in Fig.4a, a small jump in magnetization is observed in the sample with x=0, 2, 3. The main reason is that T_C^A is below the MT start temperature, and the samples do not experience an austenite ferromagnetic phase during heating and cooling. As Co content increases to 4%, ΔM associated with the structural transition further enlarges, but the peak value does not exceed 3.3 A·m²/kg. Fig.4b displays the M-T curves of the ribbons with x=5~8, and there is an obvious increase in ΔM across the MST. Due to the decrease in MT temperatures and increase in T_C^A, through the replacement of Ni with Co, the MT temperature is tuned to be lower than the T_C^A in ribbons with x=5, 6, 7, 8. Thus, a stable temperature range of ferromagnetic austenite can be obtained. In the heating process, the samples with x=5~8 experience the first-order MST from the low-magnetization martensite to ferromagnetic austenite,
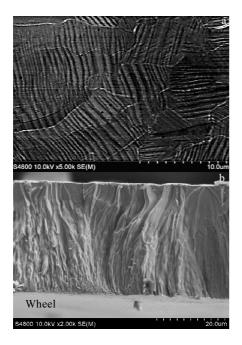
Fig.2   SEM images of the free surface of as-spun ribbons (a) and the fractured cross-section perpendicular to the ribbon plane (b)
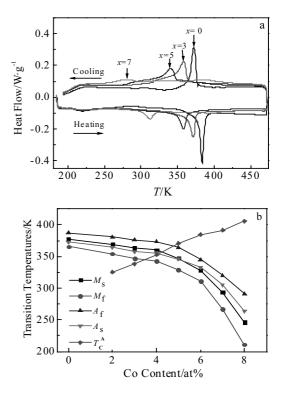
Fig.3   DSC curves (a) and composition dependence of phase transition temperatures (M_s, M_f, A_s, A_f, T_C^A) (b) for $Ni_{50-x}Co_xMn_{39}Sn_{11}$ (x=0~8) ribbons

followed by the magnetic ordering-disordering transition of austenite. The ΔM between austenite and martensite increases with increasing the content of Co. This suggests that the substitution of Co for Ni can not only modulate the MST temperature and T_C^A but also enlarge the ΔM across the martensitic transformation in these alloys. It has been reported that in Mn rich Ni-Mn-Sn alloy, the nearest Mn-Mn neighbors are introduced, which usually gives a rise to the antiferromagnetic (AFM) coupling. But the incorporation of Co atoms can be an "FM activator" and enlarge the ΔM across the MST[32, 33]. The thermal hysteresis (T_{hys}) around the MST between the heating and cooling process first gets smaller rather than getting bigger with increasing the content of Co.

Since the magnetic transition is coupled with the structural transformation in ribbons with $x=5\sim8$, the large MCE across the MST is promising. In order to analyze the MCE, isothermal magnetization (*M-H*) curves for $x=5\sim8$ samples were measured under a field up to 2400 kA/m near the RMT temperature (in heating) and MT temperature (in cooling). Before each measurement in heating, the sample is cooled to 150 K to ensure that the sample is in the martensitic state firstly. Similarly, the sample is heated to 400 K to ensure that the sample is in the austenite state before

measurement during cooling. The representative *M-H* curves of $x=6$ in the heating process are presented in Fig.5a. Obvious meta-magnetic behavior associated with a field-induced RMT from a low magnetization martensite into a high magnetization austenite can be observed. Similar meta-magnetic behavior associated with MT in cooling is also displayed in Fig.5b. According to the difference in the curves between heating and cooling, there is an obvious hysteretic loss in the magnetization and demagnetization (closed loop) during the heating process, but nearly no hysteretic loss occurs in cooling. The magnetic entropy change ΔS as a function of temperature and magnetic field for the $x=5\sim8$ alloy is calculated from the isothermal magnetization curves using the Maxwell's equation:

$$\Delta S_M(T, H_0) = \int_0^{H_0} \left[\frac{\partial M(T, H)}{\partial T}\right]_H dH \qquad (1)$$

The temperature dependences of ΔS_M for $Ni_{44}Co_6Mn_{39}Sn_{11}$ under applied fields (ΔH) of 800, 1600, and 2400 kA/m during heating and cooling is shown in Fig.6a and 6b, respectively. The maximum values of ΔS_M in RMT and MT are 18.5 and 11.1 $J \cdot kg^{-1} \cdot K^{-1}$ under the applied field of 2400 kA/m, respectively. Another important parameter for assessing the magneto-caloric behavior is the refrigerant capacity (*RC*), which estimates the amount of thermal energy that can

Fig.4 *M-T* curves for $Ni_{50-x}Co_xMn_{39}Sn_{11}$ ($x=0, 2, 3, 4$) ribbons (a) and $Ni_{50-x}Co_xMn_{39}Sn_{11}$ ($x=5, 6, 7, 8$) ribbons (b) measured during heating and cooling under a field of 8 kA/m after zero field cooling
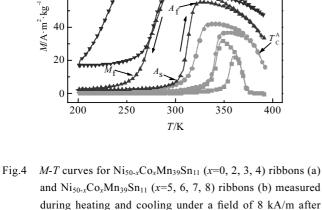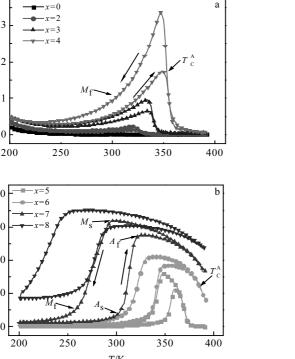

Fig.5 Isothermal magnetization curves for $x=6$ ribbons during heating (a) and cooling (b) within the transition region

be transferred by the magnetic refrigerant between the cold and hot sinks in an ideal thermodynamic cycle. *RC* values are usually determined by numerically integrating the ΔS_M-*T* curves over the full width at half maximum. The ΔS_M and *RC* of *x*=5, 6, 7, 8 ribbons are shown in Table 1. The *RC* value of RMT and MT for *x*=6 ribbons was determined to be 86.1 and 94.8 J/kg under the field changing of 2400 kA/m, respectively. As shown in Table 1, under a field change of 2400 kA/m, the maximum value of ΔS_M for *x*=7 alloy in RMT is 12.5 J·kg^{-1}·K^{-1} which is lower than 18.5 J·kg^{-1}·K^{-1} for *x*=6 ribbons, but the *RC* value is larger than that of *x*=6 alloy. Thus, broadening the transformation width is also an effective means to gain large MCE[34].

For further evaluating the usefulness of the magnetic refrigerant during a thermodynamic cycle, the hysteresis loss should be subtracted. The hysteresis loss can be estimated from the area between the field-up and field-down magnetization curves recorded at different temperatures. As shown in the insets of Fig.6a and 6b, the values of the average hysteresis loss are 13.6 J/kg in RMT and 1.3 J/kg in MT for *x*=6 samples under a field change of 2400 kA/m. After subtracting the average hysteresis loss, the effective
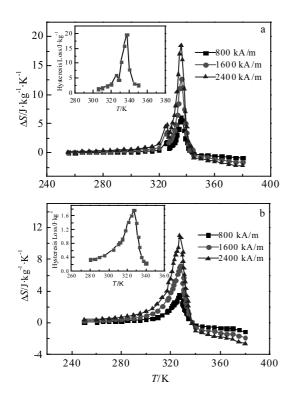
Table 1 ΔS_M, RC^{1st} and RC_{eff} for Ni$_{50-x}$Co$_x$Mn$_{39}$Sn$_{11}$ (*x*=5, 6, 7, 8) alloys under different magnetic fields at the RMT temperature

x	ΔS_M/J·kg^{-1}·K^{-1} (800/1600/2400 kA/m)	RC^{1st}/J·kg^{-1} (2400 kA/m)	RC_{eff}/J·kg^{-1} (2400 kA/m)
5	3.7/8.0/13.0	84.78	74.7
6	6.2/12.7/18.5	86.10	72.5
7	4.1/8.1/12.5	94.70	82.3
8	3.3/7.2/11.2	79.63	69.8

refrigerant capacity (RC_{eff}) of RMT and MT was determined to be 72.5 J/kg and 93.5 J/kg, respectively.

Fig.7 displays the *M-T* curves of Ni$_{44}$Co$_6$Mn$_{39}$Sn$_{11}$ ribbons measured in various magnetic fields during heating and cooling. Under a field of 2400 kA/m, the MT temperatures are found to shift to the lower temperature region at a rate of 3.35 K/T compared to under a lower magnetic field environment. This behavior suggests that when a magnetic field is applied in the vicinity of the A_s, the RMT from martensite with low magnetization to austenite with high magnetization can be induced due to the strong magneto-structural coupling in Ni$_{44}$Co$_6$Mn$_{39}$Sn$_{11}$ ribbons. The reduction of the A_s induced by the magnetic field in the present work can be well described by the Clausius-Clapeyron equation, $\Delta H/\Delta T=\Delta S_M/\Delta M$, where ΔS and ΔM stand for the differences in entropy and magnetization between austenite and martensite phases, respectively. Here, ΔM reaches 53.6 A·m^2/kg under the field of 2400 kA/m, and $\Delta H/\Delta T$ was determined to be about 3.35 K/T from the *M-T* curves. Around the MT temperature, the maximum value of ΔS_M is 16.0 J·kg^{-1}·K^{-1} for the magnetic field of 2400 kA/m according to the Clausius-Clapeyron equation, which is lower than the value of 18.6 J·kg^{-1}·K^{-1} calculated by Maxwell's method.
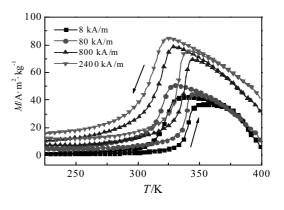

Fig.6   Temperature dependence of ΔS under a field of 800, 1600, and 2400 kA/m during heating (a) and cooling (b) processes within the transition region of *x*=6 ribbons (insets show the hysteresis losses at 2400 kA/m)

Fig.7   *M-T* curves for Ni$_{44}$Co$_6$Mn$_{39}$Sn$_{11}$ ribbons upon heating and cooling in the magnetic fields of 8, 80, 800, and 2400 kA/m

3　Conclusions

1) For $Ni_{50-x}Co_xMn_{39}Sn_{11}$ (x=0~8) ribbons, the MT temperature decreases progressively and the T_C^A continuously increases with the increase in Co content, since the valence electron number decreases with the substitution of Co for Ni.

2) For $Ni_{50-x}Co_xMn_{39}Sn_{11}$ (x=2~4) ribbons, there is no obvious ΔM around MT temperature since the MT occurs from paramagnetic austenite to weak magnetic martensite. In ribbons with x=5~8, the MT occurs from ferromagnetic austenite to weak magnetic martensite. Owing to the large ΔM between austenite and martensite, the RMT can be induced by the magnetic field, and a large MCE is obtained.

3) The maximum ΔS_M reaches 18.5 and 11.1 J·kg^{-1}·K^{-1} for RMT and MT under a field change of 2400 kA/m, respectively. After subtracting the average hysteresis loss of 13.6 J/kg in the RMT and 1.4 J/kg in the MT, the effective refrigerant capacity RC_{eff} of RMT and MT for $Ni_{44}Co_6Mn_{39}Sn_{11}$ ribbons is 72.5 and 93.5 J/kg under a field change of 2400 kA/m, respectively.

References

1　Shen B G, Sun J R, Hu F X *et al. Advanced Materials*[J], 2009, 21(45): 4545

2　Pecharsky V K, Gschneidner K A. *Phys Rev Lett*[J], 1997, 78(23): 4494

3　Engelbrecht K, Nielsen K K, Bahl C R H *et al. Journal of Applied Physics*[J], 2013, 113(17): 3673

4　Hadimani R L, Melikhov Y, Schlagel D L *et al. Journal of Applied Physics*[J], 2015, 117(17): 683

5　Campos A D, Luz M S D, Campos A D *et al. Journal of Magnetism & Magnetic Materials*[J], 2015, 374: 342

6　Fujita A, Fujieda S, Fukamichi K. *Journal of Applied Physics*[J], 2006, 99(8): 4756

7　Ito W, Imano Y, Kainuma R *et al. Metallurgical and Materials Transactions A*[J], 2007, 38(4): 759

8　Wu Zhigang, Liu Zhuhong, Yang Hong *et al. Applied Physics Letters*[J], 2011, 98(6): 262 504

9　Han Zhida, Chen Jie, Qian Bin *et al. Scripta Materialia*[J], 2012, 66(2): 121

10　Chen F, Liu W L, Shi Y G *et al. Journal of Magnetism & Magnetic Materials*[J], 2015, 377: 137

11　Liao Pan, Jing Chao, Zheng Dong *et al. Solid State Communications*[J], 2015, 217: 28

12　Jing Chao, Liu Yang, Zheng Dong *et al. Solid State Communications*[J], 2016, 241: 32

13　Zhang Xuexi, Qian Mingfang, Zhang Zhe *et al. Applied Physics Letters*[J], 2016, 108(5): 052 401

14　Sielicki K, Wróblewski R, Leonowicz M. *Acta Physica Polonica*[J], 2015, 127(2): 644

15　Jing C, Yang Y J, Li Z *et al. Journal of Applied Physics*[J], 2013, 113(17): 4358

16　Khan M, Dubenko I, Stadler S *et al. Applied Physics Letters*[J], 2013, 102(11): 219

17　Han Z D, Wang D L, Zhang C L *et al. Materials Science & Engineering B*[J], 2009, 157(1): 40

18　Gao Zhiyong, Chen Baishu, Meng Xianglong *et al. Journal of Alloys & Compounds*[J], 2013, 575(8): 297

19　Chen Jie, Qian Bin, Zhang Ping *et al. Journal of Magnetism & Magnetic Materials*[J], 2011, 323(2): 248

20　Li Z, Xu K, Yang H M *et al. Journal of Applied Physics*[J], 2015, 117(22): 233 201

21　Chen Fenghua, Gong Changwei, Guo Yanping *et al. Physica Status Solidi*[J], 2013, 210(12): 2762

22　Chen Fenghua, Gong Changwei, Guo Yanping *et al. Chinese Physics B*[J], 2014, 23(6): 514

23　Feng W J, Zuo L, Li Y B *et al. Materials Science & Engineering B*[J], 2011, 176(8): 621

24　Sutou Y, Imano Y, Koeda N *et al. Applied Physics Letters*[J], 2004, 85(19): 4358

25　Krenke T, Acet M, Wassermann E F *et al. Physical Review B Condensed Matter*[J], 2005, 72(1): 727

26　Zheng Hongxing, Wang Wu, Xue Sichuang *et al. Acta Materialia*[J], 2013, 61(12): 4648

27　Aydogdu Y, Turabi A S, Kok M *et al. Journal of Alloys & Compounds*[J], 2016, 683: 339

28　Jiang Yiwen, Li Zongbin, Li Zhenzhuang *et al. European Physical Journal Plus*[J], 2017, 132(1): 42

29　Mañosa L, Moya X, Planes A *et al. Applied Physics Letters*[J], 2008, 92(1): 1966

30　Chen Fenghua, Huang Qingxue, Jiang Zhengyi *et al. Smart Materials & Structures*[J], 2016, 25(5): 055 031

31　Moya X, Mañosa L, Planes A *et al. Materials Science & Engineering A*[J], 2006, 438: 911

32　Kainuma R, Ito W, Umetsu R Y *et al. Applied Physics Letters*[J], 2008, 93(9): 1966

33　Ma L, Zhang H W, Yu S Y *et al. Applied Physics Letters*[J], 2012, 100(15): 4358

34　Cugini F, Porcari G, Fabbrici S *et al. Philosophical Transactions*[J], 2016, 374(2074): 20 150 306

Ni$_{50-x}$Co$_x$Mn$_{39}$Sn$_{11}$ 合金薄带的微观结构，马氏体相变和磁热性质研究

张敏刚 [1]，李少波 [1]，陈峰华 [1]，张 稳 [1]，李 帆 [1]，许小红 [2]，刘建生 [1]

(1. 太原科技大学，山西 太原 030024)

(2. 山西师范大学，山西 临汾 041004)

摘 要：用单辊溶体快淬法制备了一系列的 Ni$_{50-x}$Co$_x$Mn$_{39}$Sn$_{11}$ (x=0~8) 合金薄带，并研究了它的晶体结构、相转变和磁热效应。结果表明：随着 Co 对 Ni 取代量的增加，马氏体转变温度下降明显，居里温度呈线性增加。马氏体结构转变不仅可以通过温度来诱发，也可以通过磁场来驱动。磁场强度为 2400 kA/m 时，在升温和降温过程均得到了大的磁熵变和磁制冷能力值，并且在降温过程的磁滞损耗很低。

关键词：Ni-Co-Mn-Sn合金；马氏体相变；磁热性质；磁熵变

作者简介： 张敏刚，男，1962 年生，博士，教授，太原科技大学材料科学与工程学院先进材料研究所，山西 太原 030024，E-mail: am_lab@yeah.net